Progress In Electromagnetics Research B, Vol. 9, 53–68, 2008

OPTIMIZATION AN ANECHOIC CHAMBER WITH RAY-TRACING AND GENETIC ALGORITHMS

S. M. J. Razavi and M. Khalaj-Amirhosseini

College of Electrical Engineering
Iran University of Science and Technology
Tehran, Iran

Abstract—Anechoic chambers are used for both emission and immunity testing but the ferrite tiles used to line the inside of the chamber are extremely expensive. This paper describes a method of reducing the number of tiles, whilst ensuring a reliable test environment.

In this paper, the ray-tracing method for waves propagation is used for evaluation of the reflectivity level of an anechoic chamber, and genetic algorithms are used. And use genetic algorithms to optimize the layout of ferrite tile absorber in a partially lined enclosure to produce a best performance.

The results show that it is possible to cover just 80% of the surface of the enclosure with ferrite absorber and obtain good agreement by fully lined enclosure with an error of less than 3 percent over the whole test points.

1. INTRODUCTION

The need for indoor testing of electromagnetic radiating devices, which began in the early 1950s [1], has led to a number of companies providing chambers and absorber products supporting a range of electromagnetic testing requirements. Microwave anechoic chambers are currently in use for a variety of indoor antenna measurements, electromagnetic interface (EMI) measurements, and electromagnetic compatibility (EMC) measurements [2]. The mentioned chambers provide sufficient volume for an antenna to generate a known field. This volume is called "quiet zone" and the level of reflected waves within it determines the performance of the anechoic chamber.

The large demand for testing in the 30 to 1000 MHz frequency range has brought about the development of series of materials

optimized for this application. The most common material is ferrite tile. The ferrite tiles are expensive and the room strength required to support the weight of the tiles (of the order of 30 kg/m) adds to the cost.

The need for decreasing the cost, led to develop some new optimized analytical and practical methods. Based On the experiments [3], with 80% of Fresnel zone absorbing coverage, the variation of the E-field is very uniform at all frequencies above 300 MHz and the maximum error is 1.4 dB. Some optimized methods by using additional absorbers and shifted absorbers and new absorber lining of optimized material are proposed in [4].

The method offered in this paper describes a new technique to reduce the need for full coverage of lining material and optimize the layout of absorbing material tiles to reach a good performance for the chamber and minimize the cost. The offered method has been simulated via computer programs and validated with CST MICROWAVE STUDIO.

The modeling technique is described in Section 2. Section 3 presents the results of this work. Conclusions are given in Section 4.

2. MODELING TECHNIQUE

In first step the reflectivity level of an anechoic chamber is evaluated for dipole antenna using the ray-tracing method. The method is described in subsection 2.1. The next step is explained the genetic algorithm to optimize the layout of ferrite tile absorber in a partially lined enclosure to produce best performance. The algorithm is described in subsection 2.2. The model of ferrite tile in the wide frequency range is described in subsection 2.3.

2.1. Ray-Tracing Method

The waves from a transmitting antenna can be modeled as many ray tubes shooting from the location of the antenna [5]. In our ray-tracing program, every ray tube is composed of four rays defined by the increments of θ and ϕ ($\Delta\theta$ and $\Delta\phi$) in local spherical coordinates centered at the antenna and the ray tubes have about the same solid angle to improve program efficiency. To generate those ray tubes, a sphere of radius r centered at the antenna is divided into quadrilateral cells that are close to squares with approximately the same area by selecting a fixed $\Delta\theta$ and $\Delta\phi$ a about equal to $\Delta\theta/\sin\theta$. The value of θ at the center of each cell may be used to determine $\Delta\theta/\sin\theta$, which is then adjusted for $\Delta\phi$ to obtain an integer number of cells

along the ϕ. Coordinate. Besides, for the dipole antenna, the axis of the dipole is chosen to be the local Y axis of the spherical coordinates so that the field strengths of the initial tubes are symmetry in ϕ and the tubes along the local Y axis can be neglected. Only the significant radiation regions need to be covered by those ray tubes, which are then traced one by one to find their GO contributions at the location of the receiving antenna.

The ray tracing technique provides a relatively simple solution for indoor wave propagation [6–9]. However, it should be noted that the application of GO is incorrect when the object of interest has the dimensions that are comparable or less than wavelength.

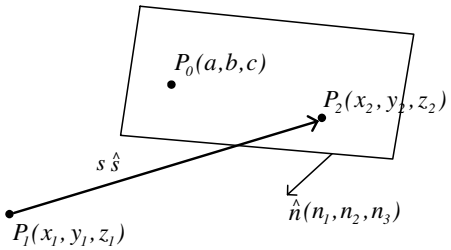

Figure 1. A ray propagates from P_1 to P_2 on an intercepting plane.

The basic ray-tracing procedure is described below.

1) Each ray of the ray tubes is traced to find an incident point (as shown in Fig. 1) where a ray propagates from a point $P_1(x_1, y_1, z_1)$ to an incident point $P_2(x_2, y_2, z_2)$ on an intercepting interface. The coordinates of the incident point P_2 can be determined from the following expression:

$$(x_2, y_2, z_2) = (x_1, y_1, z_1) + s\hat{s} \tag{1}$$

where $\hat{s}$ is the directional vector of the incident ray and s is the path length of the ray. For a flat interface defined with a normal unit vector $\hat{n} = (n_1, n_2, n_3)$ and a point $P_0 = (a, b, c)$ on the interface, the path length is given by

$$s = \frac{\hat{n} \cdot (P_0 - P_1)}{\hat{n} \cdot \hat{s}} \tag{2}$$

This is obtained from the relation $\overrightarrow{P_0P_2} \cdot \hat{n} = 0$. For a finite-size interface, it is also necessary to check whether the incident point is within the boundary of the interface or not. All interfaces that may be illuminated by the ray tube should be tested to find the incident points and the incident point with the shortest path

length from P_i is the true intercepting point. Except for the initial rays from the transmitting antenna, point P_1 is on an interface, too. Thus, for each interface that may start the ray tracing, based on the relative geometry of the structures, a list of the searching order over the other interfaces to find the incident point may be generated before starting the ray-tracing procedure to improve program efficiency.

2) When a ray tube incidents on an interface, a reflected and a transmitted ray tube is generated according to Snell's law and the local plane wave approximation. The reflection and transmission coefficients derived for a plane wave illuminating a flat interface of two materials are employed [7].

3) A ray tube will be terminated if:
   1) It exits outdoor or leaves the simulated domain;
   2) It hits any edge of the structures (i.e., diffractions are neglected);
   3) The magnitude of the E-field is less than a threshold. For 3), the total length of the ray paths from the transmitting antenna to the present location is used to approximate the spreading factor of the E-field. A Convergence test should be performed to set the proper threshold, which is defined as the percentage of the reference field strength at 1 m from the transmitting antenna. If both the reflected and transmitted rays are significant, one of the ray tubes is stored by pushing it into a "stack," while the other one is continuously traced. The data set for each stored ray tube includes the directional vectors, positions, total path lengths, and E-field phasors (excluding the spreading factor) of the four rays. If both ray tubes are ended, a previously saved ray-tube data set is then popped from the stack and the ray-tracing procedure is started again. When the stack is empty, a new initial ray tube from the transmitting antenna is traced until finished. Multiple reflections and transmissions through walls, ceiling, stairs, floors, and other electrically large bodies can be simulated both in air and in the structures to properly model wave propagation and penetration in buildings.

4) When a ray tube enters the room containing the receiving antenna, as shown in Fig. 2, a test is then performed to determine whether or not this tube passes through the receiving point R. The ray tube entering the receiving room will be composed of four rays; otherwise, the ray tube has illuminated an edge of the structures and has been terminated in 3) already. The procedure of the test is described below.

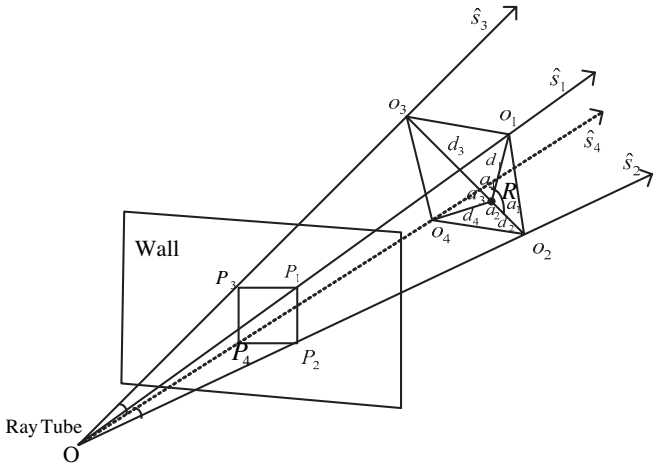

Figure 2. A ray tube passing a receiving antenna at R.

a) Find the four intercepting points O_i's of the ray-tube incident on a plane that is perpendicular to one of the four rays and contains the receiving point.
b) Determine the four angles α_i's formed O_i's and R with $0 \leq \alpha_i \leq \pi$.
c) If the sum of the four angles α_i's is less than 2π, then the ray tube does not pass through R. However, 1.999π was actually employed instead of 2π in the comparison and double precisions were used to avoid possible numerical mistakes in determining the interception. The E-field vector phasors of the tubes passing the receiving point are superposed to obtain the E-field at this field point [5]. All the field points in the receiving room may be checked and evaluated during 4) to obtain the field distributions more efficiently.

5) From the geometrical optics, the E-field of the ray tube at the receiving point can be determined from the following equation:

$$\vec{E} = \vec{E}_0 \cdot \left\{ \prod \overline{\overline{R_i}} \right\} \cdot \left\{ \prod \overline{\overline{T_i}} \right\} \cdot \left\{ \prod e^{-r_i l_i} \right\} \cdot SF \tag{3}$$

where $\overrightarrow{E}_0$ is the E-field at a reference point r_0, $\left\{ \prod \overline{\overline{R_i}} \right\}$ and $\left\{ \prod \overline{\overline{T_i}} \right\}$ are, respectively, the reflection and transmission coefficient dyads along the whole ray path, $\left\{ \prod e^{-r_i l_i} \right\}$ is the product of the propagation phase variations and exponential losses for this ray

contribution starting from r_0, and SF is the spreading factor. From the conservation of energy flux in a ray tube [7], SF can be obtained by using

$$SF = \sqrt{A_0} \Big/ \sqrt{A} \tag{4}$$

where A_0 and A are the cross-sectional areas of the ray tubes at the reference point r_0 and the field point r, respectively. The sum of the areas of the four triangles on the intercepting quadrilateral at the receiving point as shown in Fig. 2 may be evaluated to approximate the cross-sectional area A.

In this paper transmission ray tubes are attenuated and only reflection ray tubes are traced at each interface. The spreading factor is determined from the cross-sectional area of the ray tube; this ray-tube tracing method can be applied to find the reflection contribution for rather complicated structures.

2.2. Genetic Algorithm

Ferrite tiles are generally 10 cm squares. The size of anechoic chamber means that the number of 10-cm-square positions that may be occupied by a tile is of the order of 10000 (for a $9\,\mathrm{m} \times 9\,\mathrm{m} \times 10\,\mathrm{m}$ room). The room under investigation here (cover just 80% of its surface) would need approximately 417600 tiles. To search manually for the best performance in a problem of this size would be impossible. An automated system is necessary and the use of genetic algorithms is suited for this type of search.

Genetic algorithms are used to search for a solution to a problem which produces a global maximization (or minimization) of the function describing that problem [11–17]. A set of possible solutions is expressed in a way (such as a binary string) which allows them to be subject to crossover and mutation to generate a new set of possible solutions. Crossover is the swapping of two parts of the string. Before crossover is affected, the first set of possible solutions is evaluated and the results are used to select a subset upon which the crossover is carried out or all the solutions are ranked and the crossover based on this ranking. There are various ways of carrying out the selection and the crossover, as well as introducing "mutations" which increase the probability that the solution is for the global problem (not a local one) by moving the population of solutions out of local minima. The selection used for this work was the "tournament" selection in which two possible solutions are selected at random and the solution with the best cost function is chosen as a parent of the next generation.

Both possible solutions are then replaced in the population and two more solutions are selected at random (note that this may select one possible solution more than once and in fact may select good solutions many times) and one is chosen to be another parent in the same way. Tournament selection was used as it has been found to provide a faster convergence than other selection methods for a range of problems [9]. The Cost Factor was monitored during the runs and was found to tend toward the final result without any significant deviations, which implies that the algorithms used were convergent for this particular problem.

Once the parents have been selected, two parents are then "crossed over" to produce two children. In this a random section of the binary string from one parent is removed and replaced with the same part of the string from the second parent (and vice versa) to generate two "children" for the next generation. As the string in this case represented positions on the walls of the enclosure, the portions of the string which were swapped were not contiguous but were chosen to represent rectangular blocks of tiles.

To enable the work to be carried out within the time available, the problem space was reduced by dividing the surface area of the enclosure into 0.25-m squares, each one of which was either fully tiled or not tiled. The position of each square was then assigned to a point on the binary string with the 1/0 s indicating tiles/no tiles. The numbers of cells for this case (9 m × 9 m × 10 m room) are 2090 and equal by the size of string. This significantly reduced the number of possible permutations available and also simplified the problem when the tiles were installed in the enclosure.

2.3. Representing Ferrite Tiles

Ferrite tile absorbers are made of solid ferrite about 6 mm thick or in a grid construction approximately 20 mm thick. These ferrite tiles cannot be represented accurately over a wide frequency range. This is due to the change in their permeability with frequency. They can be represented using the method of [18–23] but the fine mesh required precludes room modeling due to the very large amount of computer memory required.

These problems have been partially overcome by the development, at York, of a frequency-dependent boundary which accurately models both the phase and amplitude of the reflection coefficient of solid ferrite tiles. This technique can be used with any mesh size to model the action of ferrite absorbing tiles.

The formulation is based on the observation that the frequency dependence of ferrite absorbing tiles behaves in a similar manner to

the second-order function as

$$F(s) = -\left[\frac{s^2 + 2a\omega_n s + \omega_n^2}{k(s+d)(s+e)}\right] \tag{5}$$

where s is the Laplace variable. The reflection has a minimum magnitude $\rho_{\min}$ when $s = j\omega_n$. The coefficients of the function can be determined from a few points on the reflectivity curve (magnitude only). The equation includes the pole at $s = -e$ to limit the value of reflection coefficient at high frequencies. Without this pole, the reflection coefficient could become greater than 1 at higher frequencies.

For large s

$$F(s) \approx -\left[\frac{1}{k}\right] \tag{6}$$

And as s tends to zero

$$F(s) \approx -\left[\frac{\omega_n^2}{kde}\right] \tag{7}$$

We know that the reflection coefficient for the tile tends to -1 at low frequencies so we can match the functions by taking key points on the reflectivity curve of the ferrite tile. Therefore,

$$\omega_n = 2\pi f_{\min} \tag{8}$$

where f_{min} is the frequency of the reflection minimum $\rho_{\min}$. The factor k is given by

$$k = \frac{1}{\rho_h} \tag{9}$$

where ρ_h is the magnitude of the reflection coefficient at the highest frequency part of the curve (where the reflection coefficient levels out) The pole e is then determined by

$$e = \frac{2\pi f_u}{\rho_u} \tag{10}$$

where f_u is the frequency of a point well above the reflection minimum, before the reflection coefficient levels out, and ρ_u is the magnitude of the reflection coefficient at that point.

The Damping factor a can be expressed as a function of earlier factors and the minimum value of the reflectivity $\rho_{\min}$

$$a = \frac{ke\rho_{\min}}{2\omega_n} \tag{11}$$

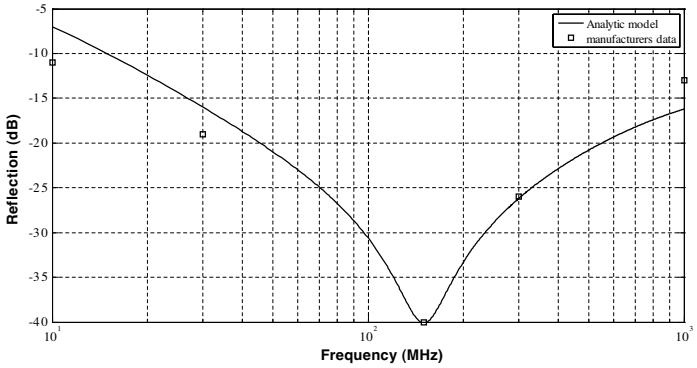

Figure 3. Modeled reflectivity curve for Philips tiles.

The pole position, d, is fixed by the fact that the reflectivity [and hence $F(s)$] must become -1 as s tends to zero so that rearranging (7) we obtain

$$d = \frac{\omega_n^2}{ke} \tag{12}$$

2.4. Settings for Optimization

Since the final aim of the work was to optimize the tile configuration with an automated computer program, a single figure of merit was required to represent the quality of each tile configuration.

The figure of merit chosen for this work was generated from the difference between the reflectivity level (RL) in the completely lined absorber anechoic chamber (RLCAC) and the RL in the partially lined absorber anechoic chamber (RLPAC). The reflectivity level, RL, of an anechoic chamber is defined as

$$\mathrm{RL} = \frac{\sum E_{Ri}}{E_{Fs}} \tag{13}$$

where E_{Ri} is the reflected field, at receiving point R, due to the ith Reflected ray and E_{Fs} is the free space field at point, R. the figure of merit is obtained by Equation (14).

$$Cost = \sum_{frequency} \sum_{testpoints} (\mathrm{RLCAC} - \mathrm{RLPAC})^2 \tag{14}$$

To keep the time taken for each model to a minimum, the grid size used was 50 cm. The waves from a transmitting antenna were modeled as 407 ray ($\Delta\theta = .1745^R$, $\Delta\varphi = .1745^R/\sin(\theta)$) tubes shooting from the location of antenna.

3. RESULTS

The anechoic chamber dimensions used were $9\,\mathrm{m} \times 9\,\mathrm{m} \times 10\,\mathrm{m}$. The positioning of the excitation and test points in the enclosure was chosen to comply with the requirements of the draft concept standard: EN 50147-3 Emission measurements in fully anechoic chambers. The position of excitation antenna was (3 m 3 m 4 m). The test points selected for optimization process is shown in Fig. 4. These points are numbered from 1 to 15 in result figures.

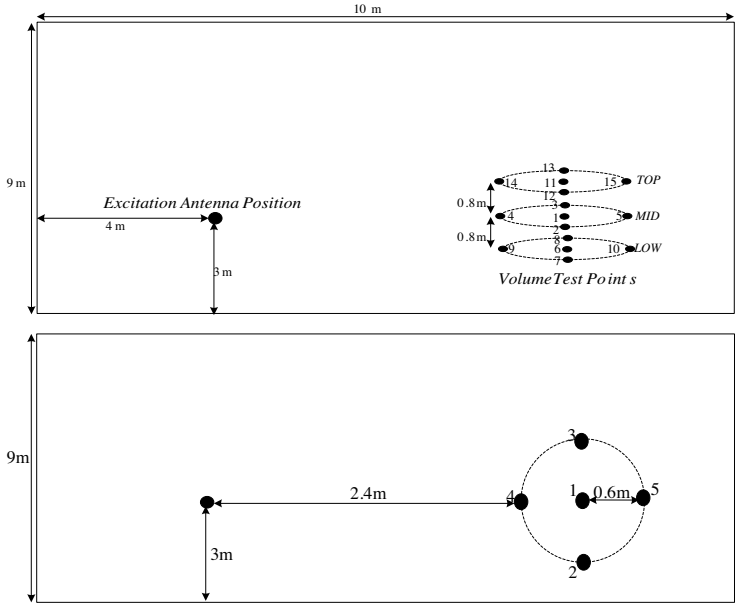

Figure 4. Positions of excitation antenna and 15 test point's volume.

The first run was for a dipole antenna at 100 MHz frequency. The optimization process was begun with 1000 generations to reduce the cost factor. The final layout for tiles was obtained after nearly 40 iterations for optimization process. This layout is shown in Fig. 5.

To validate this layout, the predicted and simulated (with CST MICROWAVE STUDIO) results were compared in Fig. 6. The agreement between predicted and CST simulated result, in partially lined absorber enclosure, is good with an error of less than 5 percent over 15 test points.

Comparison between predicted results in fully and partially lined absorber enclosure shows a good agreement with an error of less than 3 percent over the whole test points.

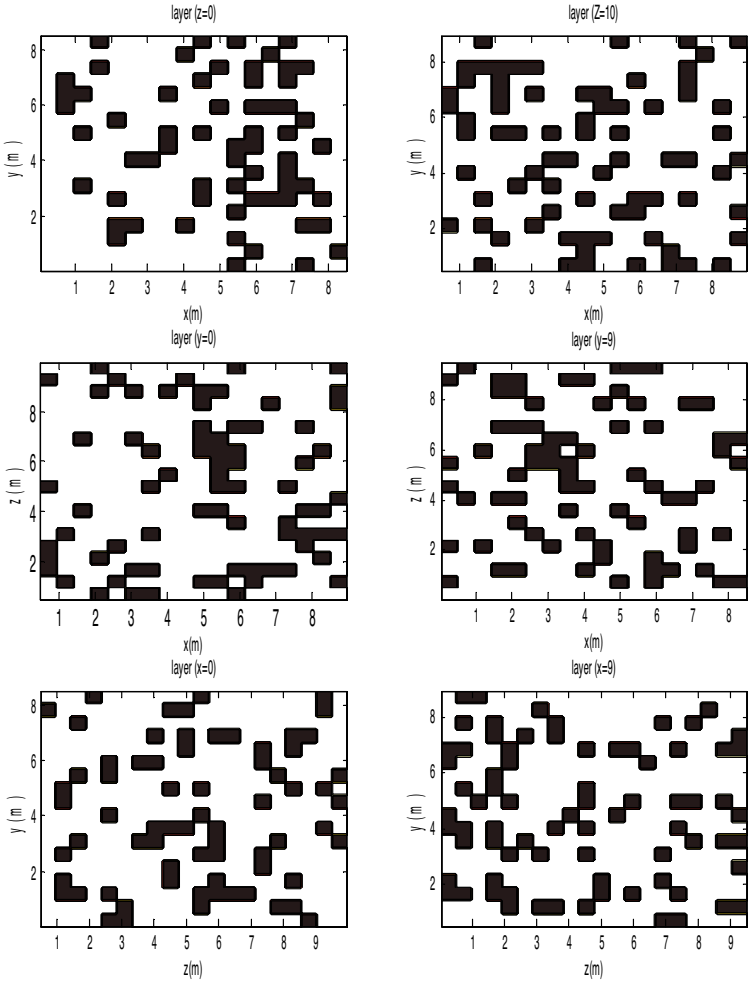

Figure 5. Optimized layout for dipole antenna excitation at 100 MHz (black = no tiles, white = tiles).

The Figs. 7 and 8 show the reflectivity level of the fully and partially lined absorber enclosure.

The maximum reflectivity level of fully lined absorber enclosure and partially lined absorber enclosure are −22 dB and −20 dB respectively. Due to good optimization, the 20% reduction of the coverage of lining ferrite tile, led to an acceptable 2 dB increase of reflectivity level of anechoic chamber. The final layout was optimized at the 100 MHz; however it is applicable for other frequency range

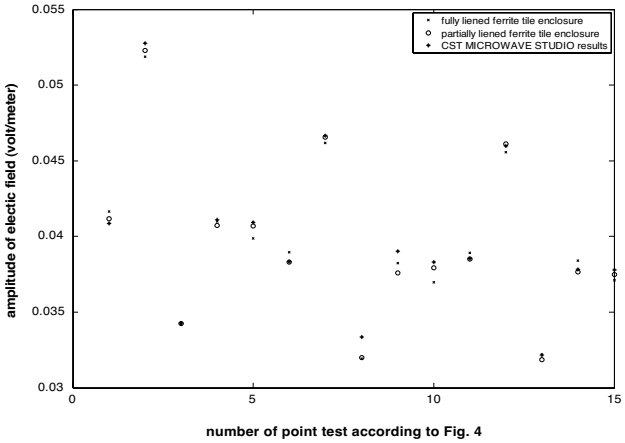

Figure 6. Compared amplitudes of electric field in the 15 test points (predicted and simulated).

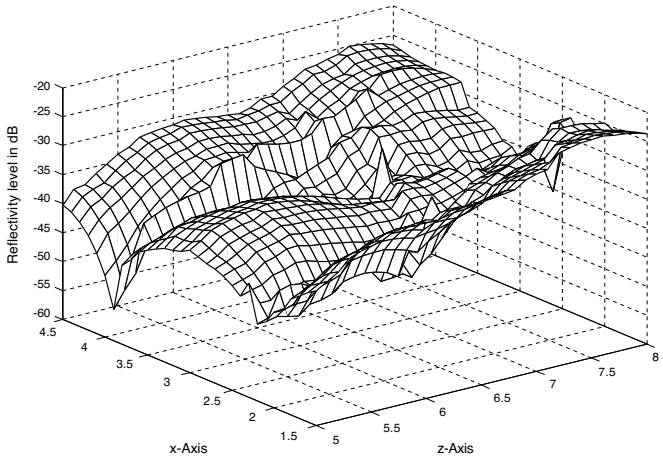

Figure 7. Reflectivity level of fully lined absorber enclosure at 100 MHz.

of ferrite tile without any change. This is due to this fact that the ray tracing algorithm is affiliated to space. The frequency range of reflectivity level of anechoic chamber is dependent on frequency of excitation antenna and frequency range of ferrite tile. The obtained layout of ferrite tiles (Fig. 5) is not offered for very long frequency range because the ray tube in the ray tracing algorithm must be narrow and frequency range of ferrite tile is limited. The Figs. 9, 10, 11 show

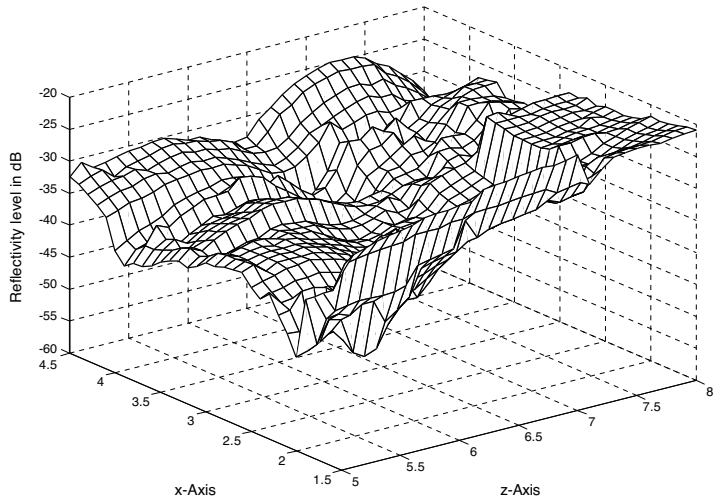

Figure 8. Reflectivity level of partially lined absorber enclosure at 100 MHz.

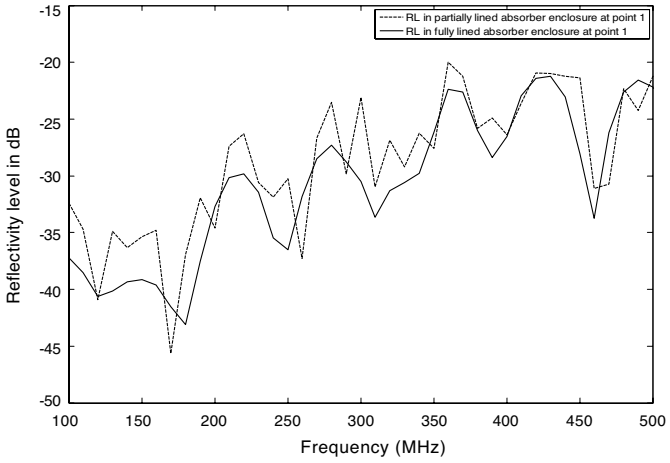

Figure 9. Compared reflectivity level of enclosure in the test point 1 at the wide frequency range.

the good result agreement between fully and partially lined absorber enclosure in the frequency range of 100–500 MHz at test point 1, 6, 11. The reflectivity level of anechoic chamber at higher frequencies (100–500 MHz) can be decreased by lining loaded carbon foam in free space between ferrite tiles.

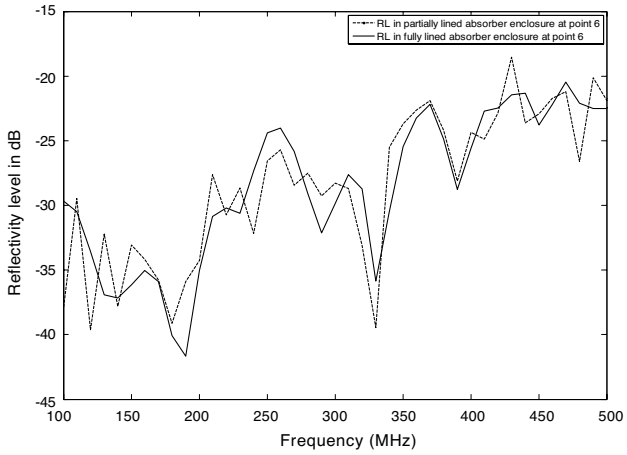

Figure 10. Compared reflectivity level of enclosure in the test point 6 at the wide frequency range.

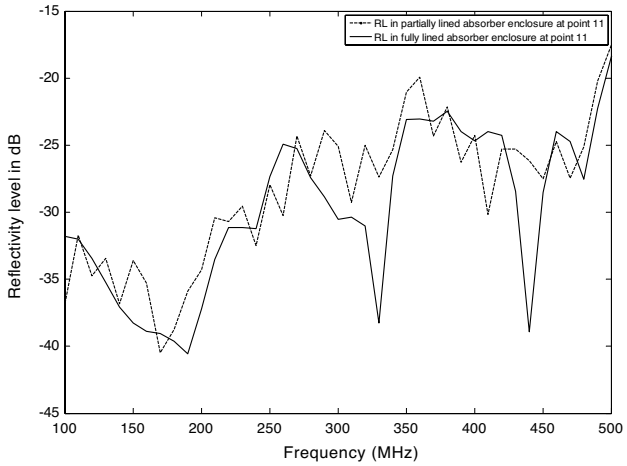

Figure 11. Compared reflectivity level of enclosure in the test point 11 at the wide frequency range.

4. CONCLUSION

This paper described a new method for optimization anechoic chambers. It is based on reduction of the coverage of lining ferrite tile to reduce the cost of an anechoic chamber and optimization of layout of absorbing material to produce a best performance. Due to

good optimization, the 20% reduction of the coverage of lining ferrite tile, led to an acceptable 2 dB increase of reflectivity level of anechoic chamber. The final obtained layout has a good performance in the frequency range 100–500 MHz.

REFERENCES

1. Emerson, W. H., "Electromagnetic wave absorbers and anechoic chambers through the years," *IEEE Transactions on Antennas and Propagation*, Vol. 21, No. 4, July 1973.
2. Marquart, N. P., "Experimental anechoic chamber measurements of a target near an interface," *Progress In Electromagnetics Research*, PIER 61, 143–158, 2006.
3. Kineros, C. and V. Ungvichian, "A low cost conversion of semi-anechoic chamber to fully anechoic chamber for RF antenna measurements," USA, 2003.
4. Bornkessel, C. and W. Wiesbeck, "Numerical analysis and optimization of anechoic chambers for EMC testing," *IEEE Trans. Electromagn. Compat.*, Vol. 38, No. 3, 499–506, August 1996.
5. Kim, H. and H. Ling, "Electromagnetic scattering from an inhomogeneous object by ray tracing," *IEEE Trans. Antennas Propagat.*, Vol. 40, 517–525, May 1992.
6. Chung, B.-K., C. H. Teh, and H.-T. Chuah, "Modeling of anechoic chamber using a beam-tracing technique," *Progress In Electromagnetics Research*, PIER 49, 23–38, 2004.
7. Jin, K.-S., T.-I. Suh, S.-H. Suk, B.-C. Kim, and H.-T. Kim, "Fast ray tracing using a space-division algorithm for RCS prediction," *Journal of Electromagnetic. Waves and Appl.*, Vol. 20, No. 1, 119–126, 2006.
8. Wang, N., Y. Zhang, and C.-H. Liang, "Creeping ray-tracing algorithm of UTD method based on nurbs models with the source on surface," *Journal of Electromagnetic. Waves and Appl.*, Vol. 20, No. 14, 1981–1990, 2006.
9. Liang, C.-H., Z.-L. Liu, and H. Di, "Study on the blockage of electromagnetic rays analytically," *Progress In Electromagnetics Research B*, Vol. 1, 253–268, 2008.
10. Balanis, C. A., *Advanced Engineering Electromagnetics*, Wiley, New York, 1989.
11. Johnson, J. M. and Y. Rahmat-Samii, "Genetic algorithms in engineering electromagnetic," *IEEE Antennas Propagat. Mag.*, Vol. 39, 7–21, August 1997.

12. Meng, Z., "Autonomous genetic algorithm for functional optimization," *Progress In Electromagnetic Research*, PIER 72, 253–268, 2007.
13. Tian, Y.-B. and J. Qian, "Ultraconveniently finding multiple solutions of complex transcendental equations based on genetic algorithm," *Journal of Electromagnetic. Waves and Appl.*, Vol. 20, No. 4, 475–488, 2006.
14. Mouysset, V., P. A. Mazet, and P. Borderies, "Optimization of broadband top-load antenna using micro-genetic algorithm," *Journal of Electromagnetic. Waves and Appl.*, Vol. 20, No. 6, 803–817, 2006.
15. Chen, X., D. Liang, and K. Huang, "Microwave imaging 3-D buried objects using parallel genetic algorithm combined with FDTD technique," *Journal of Electromagnetic Waves and Appl.*, Vol. 20, No. 13, 1761–1774, 2006.
16. Ngo Nyobe, E. and E. Pemha, "Shape optimization using genetic algorithms and laser beam propagation for the determination of the diffusion coefficient in a hot turbulent jet of air," *Progress In Electromagnetics Research B*, Vol. 4, 211–221, 2008.
17. Su, D., D.-M. Fu, and D. Yu, "Genetic algorithms and method of moments for the design of PIFAS," *Progress In Electromagnetics Research Letters*, Vol. 1, 9–18, 2008.
18. Dawson, J. F., "Improved magnetic loss for TLM," *Electron. Lett.*, Vol. 29, No. 5, 467–468, 1993.
19. Chung, B.-K. and H.-T. Chuah, "Modeling of RF absorber for application in the design of anechoic chamber," *Progress In Electromagnetics Research*, PIER 43, 273–285, 2003.
20. Dawson, J. F., "Representing ferrite absorbing tiles as frequency dependent boundaries in TLM," *Electron. Lett.*, Vol. 29, No. 9, 791–792, 1993.
21. Chamaani, S., S. A. Mirta, M. Teshnehlab, M. A. Shooredeli, and V. Seydi, "Modified multi-objective particle swarm optimization for electromagnetic absorber design," *Progress In Electromagnetics Research*, PIER 79, 353–366, 2008.
22. Khajehpour, A. and S. A. Mirtaheri, "Analysis of pyramid EM wave absorber by FDTD method and comparing with capacitance and homogenization methods," *Progress In Electromagnetics Research Letters*, Vol. 4, 123–131, 2008.
23. Abdelaziz, A. A., "Improving the performance of an antenna array by using radar absorbing cover," *Progress In Electromagnetics Research Letters*, Vol. 1, 129–138, 2008.